

Electronic structure of the quasi-one-dimensional organic conductors DCNQI (*N,N'*-dicyanoquinonediimine)-Cu salts

Akinori Tanaka, Ashish Chainani, Takayoshi Yokoya, and Takashi Takahashi
Department of Physics, Faculty of Science, Tohoku University, Aoba-ku, Sendai 980-77, Japan

Takahumi Miyazaki and Shinji Hasegawa
Institute for Molecular Science, Okazaki National Institutes, Myodaiji, Okazaki 444, Japan

Takehiko Mori

Department of Organic and Polymeric Materials, Faculty of Engineering, Tokyo Institute of Technology, Meguro-ku, Tokyo 152, Japan

(Received 17 March 1995; revised manuscript received 1 June 1995)

A comparative study of the electronic structure of *in situ* synthesized quasi-one-dimensional organic conductors (DMe-DCNQI)₂Cu and (MeBr-DCNQI)₂Cu has been carried out using various techniques of electron spectroscopy, where DMe-DCNQI and MeBr-DCNQI are 2,5-dimethyl-*N,N'*-dicyanoquinonediimine and 2,5-methylbromine-*N,N'*-dicyanoquinonediimine, respectively. From the photon-energy dependence of the valence-band photoemission spectra obtained using synchrotron radiation, the origins of each observed feature are unambiguously characterized. While the feature at the Fermi level is primarily derived from π -bonded C and N 2*p* states, the contribution of Cu 3*d* states at the Fermi level is larger in the (MeBr-DCNQI)₂Cu compared to the (DMe-DCNQI)₂Cu. X-ray photoemission spectra of the valence band imply extensive hybridization of the Cu 3*d* states with C and N 2*p* states near the Fermi level. Line-shape analyses of the Cu 2*p* core-level spectra show that the ratio of Cu²⁺ to Cu⁺ is higher in (MeBr-DCNQI)₂Cu compared to (DMe-DCNQI)₂Cu, with the ratio being closer to 1:2 for (MeBr-DCNQI)₂Cu. From a comparison of C *KVV* and Cu *LVV* Auger spectra with the self-convolution of the valence-band spectra, it is found that the effective on-site Coulomb correlation energies between the valence electrons are high on C sites as well as Cu sites in both salts, with $U(pp)=6.5$ eV and $U(dd)=8.0$ eV, respectively. In conjunction with core-level spectra, the spectra indicate that the on-site Coulomb correlation, the hybridization strength, and the charge-transfer energy between the Cu 3*d* and N 2*p* ligands are very similar in the two salts. The metal-insulator transition in (MeBr-DCNQI)₂Cu at 160 K is then facilitated by the proximity of the Cu²⁺-to-Cu⁺ ratio to 1:2 supporting charge disproportionation, while deviation from it stabilizes the metallic phase in (DMe-DCNQI)₂Cu down to very low temperatures.

I. INTRODUCTION

The series of organic conductors (2,5-*R*₁,*R*₂DCNQI)₂Cu, where DCNQI is *N,N'*-dicyanoquinonediimine and *R*₁,*R*₂=CH₃, CH₃O, Br, Cl, etc., have attracted much attention because of their interesting structural, electrical, and magnetic properties.¹⁻⁹ In these organic conductors, the π -acceptor DCNQI molecules are stacked along the tetragonal *c* axis and form the one-dimensional $p\pi$ conduction bands. Cu atoms are tetrahedrally coordinated by terminal N atoms of N-cyano group in DCNQI molecules, so that one-dimensional DCNQI columns are connected three dimensionally through Cu atoms. Therefore, some deviations from characteristic properties of a simple one-dimensional material are expected due to the interaction between $p\pi$ orbitals of DCNQI molecules and *d* orbitals of Cu ions. In fact, (DMe-DCNQI)₂Cu, where DMe is dimethyl (*R*₁,*R*₂=CH₃, CH₃), exhibits metallic behavior even at considerably low temperature (~ 50 mK), being free from the metal-insulator (MI) or Peierls transition usually observed in one-dimensional materials. Along

with other DCNQI-Cu salts which retain metallic behavior down to considerably low temperatures, it is classified as group I. In contrast, (MeBr-DCNQI)₂Cu, where MeBr is methyl-bromine (*R*₁,*R*₂=CH₃, Br), shows a sharp MI transition at 160 K accompanied by a tripling of the unit cell along the *c* axis. The DCNQI-Cu salts which show this characteristic charge-density-wave (CDW) formation at the MI transition are categorized as group II. An important difference in the salts belonging to these two groups is that the group-I salts show Pauli paramagnetism down to low temperatures, while the group-II salts exhibit local-moment formation at the MI transition which quite often results in magnetic ordering at still lower temperatures.¹⁰ Another interesting property of (DMe-DCNQI)₂Cu is the appearance of a reentrant MI transition (metal-insulator-metal transition) as a function of temperature, due to the selective replacement of hydrogen sites with deuterium atoms.^{11,12}

In this work, we have carried out a comparative study of (DMe-DCNQI)₂Cu and (MeBr-DCNQI)₂Cu as prototypes of group-I and group-II salts using various electron spectroscopic techniques. Photoemission spectroscopy

has been used to study the electronic structure and chemical states (valence) of Cu ions in these salts by other groups, but to our knowledge there is no report of a comparative study to date which highlights the differences between group-I and group-II salts. In this paper, we report the results of ultraviolet photoelectron spectroscopy (UPS), x-ray photoelectron spectroscopy (XPS), and Auger electron spectroscopy (AES) for (DMe-DCNQI)₂Cu and (MeBr-DCNQI)₂Cu. Since the photoelectron spectroscopy is very surface sensitive, we synthesized the DCNQI-Cu salts *in situ* and carried out the electron spectroscopies without exposing the samples to air. From these results, we discuss the differences in electronic structure between group-I and group-II salts that lead to their different electrical and magnetic properties.

II. EXPERIMENT

(DMe-DCNQI)₂Cu and (MeBr-DCNQI)₂Cu samples for photoemission measurements with synchrotron radiation were synthesized in a vacuum glove box filled with nitrogen gas and connected directly to the photoemission measurement system. XPS, UPS (using a He I resonance line), and AES measurements were carried out on samples made in a nitrogen-filled glove bag connected to the fast entry lock of the photoelectron spectrometer. The prepared samples were then transferred into the photoemission analysis chamber without exposure to air. The x-ray-diffraction measurements of our synthesized black fiberlike crystals showed patterns identical to those of single crystals of (DMe-DCNQI)₂Cu and (MeBr-DCNQI)₂Cu grown by the diffusion method. The details of the sample synthesis and characterization have been reported recently.¹³

Photoemission measurements using synchrotron radiation were carried out at UVSOR, Institute for Molecular Science, Okazaki, Japan. The synchrotron radiation from the UVSOR ring is monochromatized by a plane-grating monochromator. The exciting photon energy used in this experiment ranged from 20 to 75 eV. The base pressure of the analysis chamber was better than $8-9 \times 10^{-10}$ Torr. The total-energy resolution was about 150 meV.

XPS, AES, and additional UPS measurements were performed using a ESCALAB Mk II (VG Scientific Co.) photoelectron spectrometer with Al *K* α ($h\nu=1486.6$ eV) and the He I resonance line ($h\nu=21.2$ eV) as the excitation sources. The base pressure of the analysis chamber was $8-9 \times 10^{-10}$ Torr. The total-energy resolutions for XPS and UPS measurements were about 1.1 eV and 100 meV, respectively.

All measurements reported here were recorded at room temperature. The spectra showed no change in the course of the measurements but broadened considerably on air-exposure oxidation. Thus the contamination of the sample surface was monitored by the presence of O 1s signal which was negligible throughout the measurements, as well as the width of the Cu 2p core-level spectra, which is narrower than spectra reported to date. The Fermi level of the sample was determined by comparison

with a gold or silver reference. Part of the results have been reported recently by us.¹³

III. RESULTS AND DISCUSSION

A. Valence-band spectra

Figure 1 shows the photon-energy dependence ($h\nu=20-75$ eV) of the valence-band spectra obtained using synchrotron radiation for (DMe-DCNQI)₂Cu. The photoemission spectra show two major structures, positioned around 3–4 and 7.5-eV binding energy. All spectra in Fig. 1 have been normalized by the intensity of the feature at 7.5-eV binding energy. The relative intensity of these two features changes systematically as a function of the photon energy. This systematic change of the relative intensity of the two bands is due to the photon-energy dependence of the photoionization cross section of the constituent atomic orbitals. The relative photoionization cross section of Cu 3d electrons to C or N 2p electrons increases with increasing photon energy.¹⁴ This indicates that the band around 3–4 eV in the valence-band spectra is primarily derived from Cu 3d states, while that around 7.5 eV originates in the C and N 2p-derived states. This assignment of bands is consistent with ex-

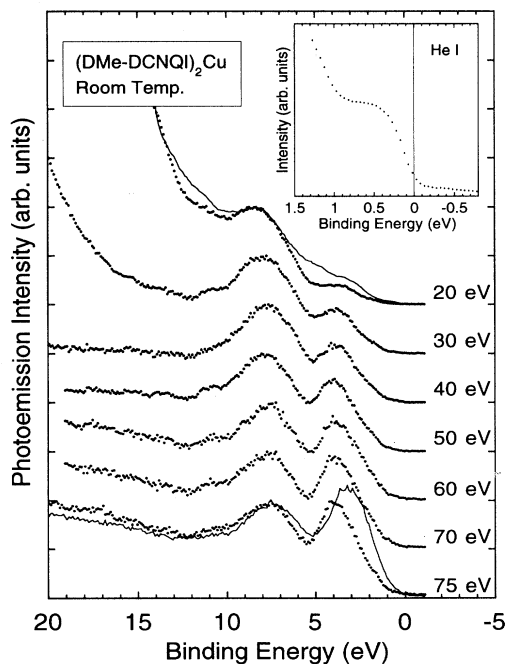


FIG. 1. Valence-band photoemission spectra of (DMe-DCNQI)₂Cu measured at room temperature as a function of incident photon energy using synchrotron radiation. Photon energies used are indicated on each spectrum. All spectra are normalized by the intensity of the feature of 7.5-eV binding energy. The inset shows the photoemission spectrum in the vicinity of the Fermi level measured by the He I resonance radiation ($h\nu=21.2$ eV) at room temperature. Valence-band spectra with $h\nu=20$ and 75 eV for (MeBr-DCNQI)₂Cu are superimposed as solid line spectra.

tended Hückel molecular-orbital calculations,¹⁵ which predict that the Cu $3d$ -derived states appear at about 3–4 eV while the C and N $2p\sigma$ -derived states originating in the quinone ring are located at about 7.5 eV. It is noted that the band around 3–4 eV, which is attributed to the Cu $3d$ states, appears in the spectra at a sufficiently low photon energy of 20 eV, though the photoionization cross section of Cu $3d$ electrons is considerably reduced at that energy. This is because the band around 3–4 eV in the low-photon-energy spectra receives substantial contributions from the C and N $2p$ -derived states of the cyano group in a DCNQI molecule, as is known from the extended Hückel molecular-orbital calculations.¹⁵ The valence-band photoemission spectra for (MeBr-DCNQI)₂Cu show similar features as well as photon-energy dependence, and the above discussion holds equally well for it.

The existence of a clear metallic Fermi edge in the photoemission spectra of low-dimensional inorganic and organic systems is an issue of major current interest. For the DCNQI salts, Schmeißer and co-workers^{16–19} reported a sharp rise in the photoemission intensity near the Fermi level, which they ascribed to the metallic Fermi edge similar to that in ordinary metals, while Inoue *et al.*²⁰ reported a smooth increase of photoemission intensity for the Fermi level in DCNQI-Cu salts which is characteristic of one-dimensional conductors like TTF-TCNQ (Refs. 21 and 22) and K_{0.3}MoO₃. In the inset of Fig. 1, we plot the photoemission spectra near the Fermi level obtained with a high signal-to-noise ratio on an expanded energy scale for (DMe-DCNQI)₂Cu. The spectrum was obtained using the He I resonance line ($h\nu=21.2$ eV) with a total-energy resolution of about 100 meV. The photoemission spectrum near the Fermi level for (MeBr-DCNQI)₂Cu is almost identical to that of (DMe-DCNQI)₂Cu. A low intensity feature within 1 eV of the Fermi level is clearly observed with a small but finite intensity at the Fermi level. This feature is derived from C and N $2p\pi$ -bonded states and straddles the Fermi level, causing the metallic behavior in these systems. An important point to note is that the leading edge in the spectra is not the Fermi edge, with the midpoint of the steep slope being away from the Fermi level. This probably indicates that the quasi-one-dimensionality of the metallic phase modifies the spectral function at the Fermi level, as is well known in other quasi-one-dimensional systems mentioned above. However, if there is a three-dimensional Fermi surface originating in Cu $3d$ orbitals in addition to the one-dimensional Fermi surface of the DCNQI molecules stacks as reported in recent de Haas–van Alphen measurements,^{24,25} a sharp Fermi-edge cutoff should exist to account for the three-dimensional Fermi surface. High-resolution with low-temperature photoemission measurements would be necessary to establish this possibility for the DCNQI-Cu salts.

Despite the above-described similarities in the valence-band spectra for (DMe-DCNQI)₂Cu and (MeBr-DCNQI)₂Cu, there are two important differences in the spectra. To highlight these differences, we have superimposed the valence-band spectra with $h\nu=20$ and 75 eV for (MeBr-DCNQI)₂Cu as solid lines in Fig. 1. The

valence-band spectrum with $h\nu=20$ eV for (MeBr-DCNQI)₂Cu exhibits an additional structure centered around 4.5 eV which is absent in (DMe-DCNQI)₂Cu. Also, it quickly reduces in intensity on increasing the photon energy, and is not observed for a photon energy of 40 eV. This additional structure in (MeBr-DCNQI)₂Cu is ascribed to the Br $4p$ states, since the photoionization cross section of the Br $4p$ electrons is comparable or larger than that of the C or N $2p$ electrons at this photon energy. The more important difference is the energy position of the Cu $3d$ -derived band, which is about 4.0 eV for (DMe-DCNQI)₂Cu and about 3.0 eV for (MeBr-DCNQI)₂Cu. This would imply a larger contribution of Cu $3d$ states at the Fermi level, and the higher amount of charge transfer from the Cu ions to the DCNQI molecules stacks in the (MeBr-DCNQI)₂Cu compared to the (DMe-DCNQI)₂Cu. As will be discussed further below, this is consistent with the differences obtained in the valence-band XPS and Cu $2p$ core-level XPS spectra of the two salts.

Figure 2 shows the valence-band XPS spectra measured at room temperature for (DMe-DCNQI)₂Cu (lower) and (MeBr-DCNQI)₂Cu (upper) excited by Al $K\alpha$ radiation ($h\nu=1486.6$ eV). These spectra are normalized by the maximum intensity. The spectrum for (DMe-DCNQI)₂Cu shows a low intensity feature at about 7.5 eV corresponding to the C and N $2p\sigma$ -derived states as seen in the spectra with low photon energies. The broad peak with higher intensity centered at about 2 eV is derived from primarily Cu $3d$ states, though the valence-band spectra at lower photon energies consist of two features around 4 and 0.5 eV. The larger width (nearly 4 eV) in the XPS spectrum compared to the UPS spectra indicates that Cu $3d$ states are strongly hybridized with the C and N $2p$ states. In the valence-band XPS spectrum for (MeBr-DCNQI)₂Cu, an additional feature at about 4-eV binding energy is observed, and is ascribed to

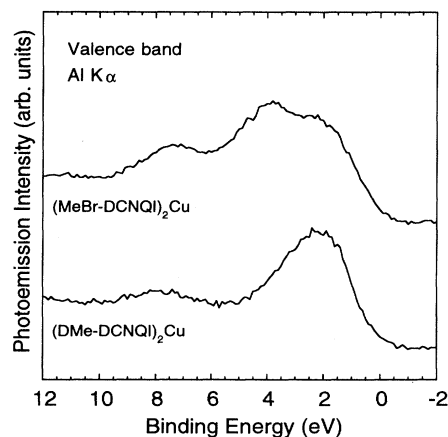


FIG. 2. Valence-band x-ray photoemission (XPS) spectra of (DMe-DCNQI)₂Cu (lower) and (MeBr-DCNQI)₂Cu (upper) measured with Al $K\alpha$ radiation ($h\nu=1486.6$ eV) at room temperature. Both spectra are normalized by the maximum intensity.

the Br 4*p*-derived states as is also seen in the UPS spectra. This is because the relative photoionization cross section of Cu 3*d* and Br 4*p* electrons to C or N 2*p* electrons is large at this high photon energy, and thus result in dominating the valence-band XPS spectra. If we normalize the spectra at the primarily Cu 3*d*-derived feature, we obtain the higher intensity at the Fermi level in the (MeBr-DCNQI)₂Cu, implying higher charge transfer. Contribution of the Cu 3*d* orbitals to the density of electronic states at the Fermi level plays a crucial role in the valence fluctuation model, as the MI transition is accompanied by a sharp change of the magnitude susceptibility in group-II salts. Schmeißer and co-workers^{16–19} performed photon-energy-dependent photoemission studies for various DCNQI-Cu salts with and without *d* orbitals at the central atoms, and thereby concluded that the top-most bands in the vicinity of the Fermi level in metallic DCNQI-Cu salts consists of a mixture of C and N 2*p*-derived states with negligible contribution from the Cu 3*d* orbitals. On the other hand, Inoue *et al.*²⁰ proposed a significant contribution from the Cu 3*d* orbitals to the Fermi-edge states based on their photon-energy-dependent photoemission study of (DMe-DCNQI)₂Cu, supporting the valence fluctuation model. Our results show that the intensity at and near the Fermi level is not enhanced strongly for low photon energies in both salts, while the feature around 3–4-eV binding energy reflects the photon-energy dependence of the photoionization cross section of Cu 3*d* electrons. This difference in the photon-energy dependence of the intensity shows that the states near the Fermi level have primarily C and N 2*p* π character, with the tail of the primarily Cu 3*d*-derived states extending into the π -bonded states. However, at $h\nu=1486.6$ eV of Al *K* α photon energy, the hybridization between the Cu 3*d* and C and N 2*p* states results in a broad feature nearly 4 eV wide with higher intensity at the Fermi level in the (MeBr-DCNQI)₂Cu. This difference should also reflect in the Cu 2*p* core-level XPS spectra and is discussed below.

B. Core-level spectra

Core-level XPS spectroscopy is a fairly straightforward technique compared to UPS spectroscopy in determining the valence states of atoms in materials, since the binding energies and/or the characteristic satellite structures of a specific core level give a direct indication of the valence states of atoms. Figure 3 shows the Cu 2*p* core-level XPS spectra measured at room temperature for (DMe-DCNQI)₂Cu (lower) and (MeBr-DCNQI)₂Cu (upper) excited by Al *K* α radiation ($h\nu=1486.6$ eV). In order to check the oxidation effect due to air exposure, the spectrum of (DMe-DCNQI)₂Cu exposed to air for one day is superimposed on the spectrum of clean sample in Fig. 3. The spectrum of the sample exposed to air becomes much broader, and additional intensity appears around 942 eV in binding energy. All previous XPS studies of DCNQI-Cu salts^{2,18,26,27} used Mg *K* α radiation ($h\nu=1253.6$ eV) as an excitation source. However, the XPS spectrum excited by Mg *K* α radiation produces the C *KVV* Auger structure in the Cu 2*p* core-level region, making it

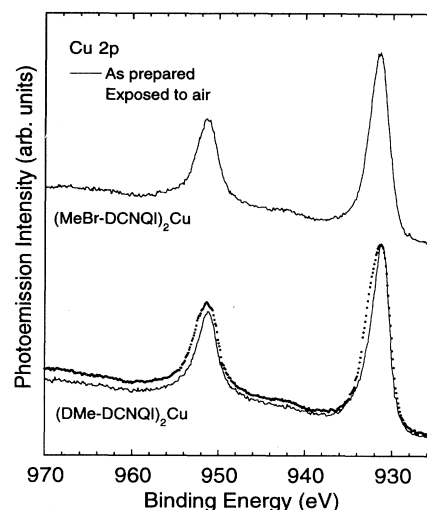


FIG. 3. Cu 2*p* core-level spectra of (DMe-DCNQI)₂Cu (lower) and (MeBr-DCNQI)₂Cu (upper) measured with Al *K* α radiation ($h\nu=1486.6$ eV) at room temperature. The dotted spectrum shows the spectrum of (DMe-DCNQI)₂Cu obtained after exposure to air.

difficult to carry out a quantitative analysis of the spectra, particularly in the Cu 2*p*_{1/2} region. In order to avoid this uncertainty due to the superposition of the C *KVV* Auger signal, we used Al *K* α radiation as the excitation source. In spite of the slightly poor natural width of the Al *K* α radiation (~ 830 meV) compared to Mg *K* α radiation (~ 680 meV), the FWHM of the Cu 2*p*_{3/2} core level is narrower than earlier reports.^{2,18,26,27}

In DCNQI-Cu salts which exhibit a MI transition at low temperature, x-ray-diffraction patterns for the insulating phases show a threefold superlattice structure, indicative of the existence of a threefold CDW. This period gives direct evidence of the mixed valence of Cu (Cu^{4/3+}); [Cu²⁺]: [Cu⁺]=1:2. However, a similar experiment (temperature dependence of x-ray diffraction) cannot yield the valence of Cu in (DMe-DCNQI)₂Cu which is free from the MI/CDW transition. Schmeißer *et al.*¹⁸ reported that there is no satellite structure due to the Cu²⁺ configuration in the Cu 2*p* core-level spectrum of *in situ* prepared (DMe-DCNQI)₂Cu. Furthermore, they found that the samples exposed to air after synthesis showed a satellite structure in the Cu 2*p* core-level spectra characteristic of Cu²⁺, and thereby concluded that the satellite structure observed in the Cu 2*p* core-level spectra in a previous report² may be due to the surface contamination produced by oxidation. On the other hand, Inoue and co-workers^{26,27} proposed that the ratio of Cu²⁺ to Cu⁺ is nearly 1:2 even in the metallic phase from a line-shape analysis of the Cu 2*p* core-level spectrum for a scraped single crystal of (DMe-DCNQI)₂Cu.

As shown in Fig. 3, the Cu 2*p* core-level spectra for both salts prepared *in situ* exhibit a narrow and slightly asymmetric peak at about 932 eV. The slight asymmetry

suggests that the Cu $2p_{3/2}$ peak consists of two components— $2p_{3/2}3d^{10}$ (Cu^+) and $2p_{3/2}3d^{10}\underline{L}$ (Cu^{2+}) final states—as has been well known.²⁸ Only the Cu^{2+} component is accompanied by a satellite structure originating from the $2p_{3/2}3d^9$ (Cu^{2+}) final state. While the satellite intensity seems negligible for $(\text{DMe-DCNQi})_2\text{Cu}$, it is clearly larger in the spectrum of $(\text{MeBr-DCNQi})_2\text{Cu}$. In order to estimate the precise contribution of each component for both salts, we carried out line-shape analyses of the Cu $2p$ core-level spectra by a least-squares method. Figures 4(a) and 4(b) show the results of line-shape analyses of Cu $2p$ core-level spectra for $(\text{DMe-DCNQi})_2\text{Cu}$ and $(\text{MeBr-DCNQi})_2\text{Cu}$, respectively. We decomposed the Cu $2p$ core-level spectra into a Cu^+ component and a Cu^{2+} component consisting of the main peak and a satel-

lite. Each peak was described by a convolution of a Lorentzian due to lifetime broadening and a Gaussian due to the instrumental broadening. Furthermore, it was found necessary to include a plasmon loss satellite at 21.4-eV higher binding energy [estimated from the electron-energy-loss spectroscopy (EELS) spectrum reported by Inoue *et al.*²⁶] to reproduce the experimental spectrum in the Cu $2p_{1/2}$ region. In Figs. 4(a) and 4(b), the long dashed lines represent the Cu^+ spectra, and the short dashed and dotted lines represent the main peak and satellite of the Cu^{2+} spectra, respectively. The difference between the observed spectra and the sum of decomposed components are also shown at the bottom. The parameters obtained from the line-shape analyses are listed in Table I for the fairly good fits shown in Figs. 4(a) and 4(b).

From the line-shape analyses of Cu $2p$ core-level spectra for $(\text{DMe-DCNQi})_2\text{Cu}$ and $(\text{MeBr-DCNQi})_2\text{Cu}$, we find that the Cu^{2+} configurations in $(\text{DMe-DCNQi})_2\text{Cu}$ and $(\text{MeBr-DCNQi})_2\text{Cu}$ are about 27% [$[\text{Cu}^{2+}]:[\text{Cu}^+] \sim 0.76:2$] and about 32% [$[\text{Cu}^{2+}]:[\text{Cu}^+] \sim 0.93:2$] in integrated intensity, respectively. These findings suggest that the ratio of Cu^{2+} to Cu^+ configurations in $(\text{DMe-DCNQi})_2\text{Cu}$ is significantly smaller than the ratio 1:2 concluded from an earlier report,^{26,27} and that the ratio in $(\text{MeBr-DCNQi})_2\text{Cu}$ is closer to 1:2. We believe that our results about the differences in the amount of Cu^{2+} configuration for both salts is precise due to the *in situ* preparation, resulting in sharper peaks and negligible contamination of the samples. This shows that the amount of charge transfer from Cu ions to the DCNQi molecules stacks in the $(\text{MeBr-DCNQi})_2\text{Cu}$ is larger than that in the $(\text{DMe-DCNQi})_2\text{Cu}$. While the energy difference between the main peak and the satellite of Cu^{2+} (10.6 eV) is slightly less than that reported earlier (11.2 eV), it is the same for both salts. Also, I_s/I_m (I_s is the satellite intensity and I_m is the main peak intensity of Cu^{2+}) is identical [0.42 and 0.43 for $(\text{DMe-DCNQi})_2\text{Cu}$ and $(\text{MeBr-DCNQi})_2\text{Cu}$, respectively] for both salts. This implies that the parameters which determine the XPS spectrum in a cluster model, namely, hybridization strength and charge-transfer energy between the Cu $3d$ and N $2p$ ligand states should have similar values for both salts, provided, of course, that the on-site Coulomb correlation energy on the Cu site is identical for both salts. This will be shown to be the case from the following analysis of the AES of both salts.

C. Auger electron spectra

In order to study the electron correlation of the valence electrons on Cu and C sites, we measured the Cu LVV and C KVV Auger spectra of both salts. Figure 5 shows the Cu LVV Auger spectra excited by Al $K\alpha$ radiation ($h\nu=1486.6$ eV) for $(\text{DMe-DCNQi})_2\text{Cu}$ (lower panel) and $(\text{MeBr-DCNQi})_2\text{Cu}$ (upper panel). Similarly, Fig. 6 shows the C KVV Auger spectra excited by Al $K\alpha$ radiation ($h\nu=1486.6$ eV) for $(\text{DMe-DCNQi})_2\text{Cu}$ (lower panel) and $(\text{MeBr-DCNQi})_2\text{Cu}$ (upper panel). The exper-

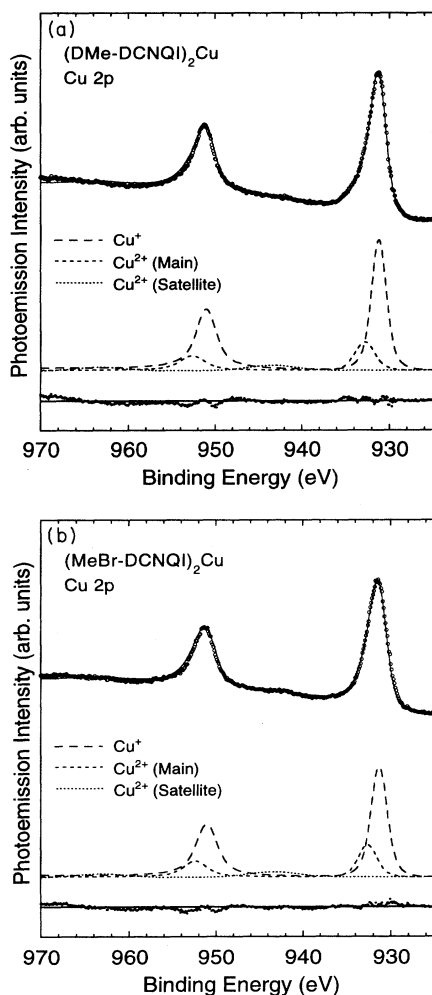


FIG. 4. (a) Result of line-shape analysis for Cu $2p$ core-level spectrum of $(\text{DMe-DCNQi})_2\text{Cu}$. The observed spectrum is decomposed into Cu^+ (long dashed line) and Cu^{2+} components (the short dashed and dotted line represent the main peak and satellite of Cu^{2+} , respectively). The bottom is the difference between the observed spectrum and the sum of the decomposed components. (b) Same as (a) but for $(\text{MeBr-DCNQi})_2\text{Cu}$.

TABLE I. Fitted parameters for the line-shape analyses of the Cu $2p$ core-level XPS spectra of (DMe-DCNQI) $_2$ Cu and (MeBr-DCNQI) $_2$ Cu. I_s is the satellite intensity, and I_m is the main peak intensity of Cu $^{2+}$.

	Binding energy (eV)	Spin-orbit splitting (eV)	$2p_{3/2}$ Lorentzian width (FWHM) (eV)	$2p_{1/2}$ Lorentzian width (FWHM) (eV)	Gaussian width (FWHM) (eV)
(DMe-DCNQI) $_2$ Cu					
Cu $^+$	931.16	19.85	0.48	1.00	1.23
Cu $^{2+}$ (main)	932.75	19.95	0.48	1.00	1.80
Cu $^{2+}$ (satellite)	943.40	19.95			5.45
(MeBr-DCNQI) $_2$ Cu					
Cu $^+$	931.30	19.75	0.48	0.99	1.38
Cu $^{2+}$ (main)	932.61	19.85	0.48	0.99	1.66
Cu $^{2+}$ (satellite)	943.30	19.85			
I_s/I_m					
(DMe-DCNQI) $_2$ Cu	0.43				
(MeBr-DCNQI) $_2$ Cu	0.42				

imental spectra are displayed using dotted lines as a function of the kinetic energy of the Auger electron, referenced to the Fermi level.

Using a three-step model for the Auger transition process, the kinetic energy of an Auger electron produced through the (jkl) transition, $E_A(jkl)$, is expressed as

$$E_A(jkl) = E_B(j) - E_B(k) - E_B(l) - U(kl), \quad (1)$$

where $E_B(i)$ is the binding energy of level i ($=j, k, l$), and $U(kl)$ is the two-hole interaction energy, which is the

effective on-site Coulomb correlation energy between the electrons in levels k and l .^{29–31} It is clear that, in the case of the Cu L_{VV} (and C K_{VV}) Auger process, the k and l levels correspond to valence-band states. Consequently, the second and third terms in Eq. (1) can be replaced by the self-convolution of the Cu $3d$ (C $2p$) valence-band partial density of states (DOS), and represents the two-hole spectrum without correlation effects.

The Cu L_{VV} Auger spectra in Fig. 5 shows the L_3VV and L_2VV features due to $2p_{3/2}$ and $2p_{1/2}$ core-level spin-orbit splitting separated by about 20 eV. The L_3VV spectrum consists of an intense feature around 916-eV kinetic energy due to the 1G atomic multiplet corresponding to the localized two-hole d^8 final state, as has also been well known for Cu metal.³² The weak feature at higher kinetic energy is due to the 3P , 1D , and 3F multiplets, and that at lower kinetic energy is the 1S multiplet. It is noted that a straightforward assignment is an oversimplification because the Auger spectra would be a composite of Cu $^+$ and Cu $^{2+}$ contributions which show a difference in kinetic-energy positions. However, since the Cu $^+$ contribution is dominant, we proceed with the analysis, as we are interested in obtaining an effective on-site Coulomb interaction only as a comparison between the two salts. The self-convolution calculation was carried out using the valence-band XPS spectrum excited by Al $K\alpha$ radiation ($h\nu = 1486.6$ eV) shown in Fig. 2, which is dominated by Cu $3d$ partial DOS due to the large photoionization cross section of Cu $3d$ electrons. The two-hole spectrum for (DMe-DCNQI) $_2$ Cu thus obtained is displayed as a solid line with respect to the zero of the two-hole energy corresponding to the Cu $2p_{3/2}$ core-level binding energy in the lower panel of Fig. 5. We find that the main peak observed in the Cu L_3VV Auger spectrum is positioned at about 8-eV lower kinetic relative to that of the calculated two-hole spectrum in (DMe-

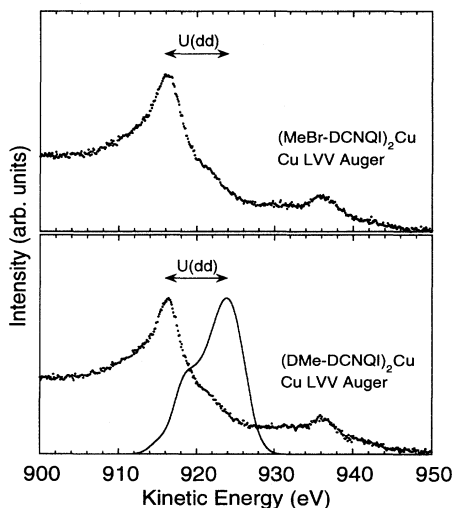


FIG. 5. Comparison of the experimental Cu L_{VV} Auger spectra (dots) with the self-convolution (solid line) of the valence-band XPS spectrum with $h\nu = 1486.6$ eV (Fig. 2) for (DMe-DCNQI) $_2$ Cu (lower panel) and (MeBr-DCNQI) $_2$ Cu (upper panel). The effective on-site Coulomb correlation energy of Cu $3d$ electrons [$U(dd)$] is estimated to be 8 eV.

DCNQI)₂Cu, and that there is negligible intensity in the experimental spectrum for the delocalized two-hole states. This energy difference of about 8 eV corresponds to the effective on-site Coulomb correlation energy of Cu 3*d* electrons, $U(dd)$, in (DMe-DCNQI)₂Cu. However, for the (MeBr-DCNQI)₂Cu, the valence-band XPS spectrum receives a large contribution from Br 4*p*-derived states which we could not subtract out meaningfully. Since the Cu 3*d*-derived states occur at the same energy position in the XPS spectrum, and the L_3VV main peak position is identical to the (DMe-DCNQI)₂Cu, we can safely estimate $U(dd)$ for the (MeBr-DCNQI)₂Cu also to be the same.

For the analyses of C KVV Auger spectra for (DMe-DCNQI)₂Cu and (MeBr-DCNQI)₂Cu, the self-convolution calculations were performed using valence-band UPS spectra of $h\nu=30$ eV, which can be considered to be most representative of the C 2*p* valence-band partial DOS because of the relatively large photoionization cross section of the C 2*p* electrons at low photon energy. We did not use the UPS spectra for $h\nu=20$ eV due to the considerably larger background from inelastic losses, which makes it difficult to extract the intrinsic spectrum. The self-convolution calculations of the valence-band spectra of $h\nu=30$ eV were carried out after subtracting a linear inelastic background. The thus-calculated two-hole spectra for (DMe-DCNQI)₂Cu and (MeBr-DCNQI)₂Cu are displayed as solid lines in the lower and upper panels of Fig. 6, respectively, and are plotted with respect to the zero of the two-hole energy corresponding to the C 1*s* core-level binding energy. As shown in Fig. 6, the observed C KVV Auger spectra for both salts exhibits a two-peak structure, with the higher kinetic feature matching well with the peak in the calculated two-hole

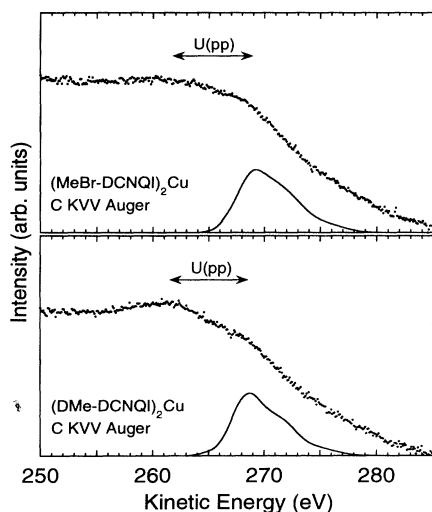


FIG. 6. Comparison of the experimental C KVV Auger spectra (dots) with the self-convolution (solid line) of the valence-band spectrum with $h\nu=30$ eV for (DMe-DCNQI)₂Cu (lower panel) and (MeBr-DCNQI)₂Cu (upper panel). The effective on-site Coulomb correlation energy of C 2*p* electrons [$U(pp)$] is estimated to be 6.5 eV.

spectra. The lower-kinetic-energy feature is then derived from atomiclike two-hole final states due to electron-electron correlations on the C site. The energy interval between the lower-kinetic-energy feature observed in the Auger spectrum and the calculated two-hole spectrum is almost the same for both salts. It represents the effective on-site Coulomb correlation energy of C 2*p* electrons, $U(pp)$, and is about 6.5 eV for both salts. This value of 6.5 eV for $U(pp)$ in both salts is rather large, but then $U(pp)$ for the oxygen 2*p* states in many oxides, including the high- T_c superconductors, is also known to be about the same value.³³ To our knowledge, this is probably the first report identifying strong on-site correlations in the C 2*p* electrons of DCNQI systems using Auger spectroscopy. In contrast, we would like to mention that recent studies on DCNQI-Ag salts have emphasized that long-ranged Coulomb interactions play an important role in those systems.³⁴

As described above, it is found for both salts that the effective on-site correlation energies between the valence electrons are fairly high on C and Cu sites, and have similar values for both salts. Our Cu L_{VV} and C KVV Auger measurements then show that the DCNQI-Cu systems can be categorized as strongly correlated electron systems, and point to an electronic origin contributing to the MI transition in DCNQI-Cu systems. In fact, recent theoretical work³⁵ has shown that the MI transition in the DCNQI-Cu salts can be considered as a cooperative CDW transition in the quasi-one-dimensional DCNQI molecules and a Mott transition in the Cu 3*d*-derived states. Our results indicate that the MI transition takes place only when the carrier concentration facilitates a charge disproportion to support a CDW. The mechanism probably originates in a superexchange-type interaction operative between nearest-neighbor Cu ions on adjacent chains through a DCNQI molecule stacks, but stabilizes the local moment on Cu sites in the insulating phase only when the system has a $\text{Cu}^+:\text{Cu}^{2+}$ ratio of 2:1. The carrier concentration or amount of charge transfer from the Cu ions to the DCNQI molecules is controlled primarily by distortion of tetrahedral coordination around Cu ions, leading to higher charge transfer in (MeBr-DCNQI)₂Cu compared to (DMe-DCNQI)₂Cu.⁶ This is consistent with recent studies³⁶ on (DMe-DCNQI-*d*₇)₂Cu_{1-x}M_x ($M=\text{Li}$ and Zn), which show that the MI transition can be suppressed with Li^+ substitution while Zn^{2+} substitution increases the MI transition temperature. This is exactly the situation for (DMe-DCNQI)₂Cu and (MeBr-DCNQI)₂Cu. Recent optical measurements³⁷ have also shown that (DMe-DCNQI)₂Cu retains metallic conductivity along the *c* axis as well as in the plane perpendicular to it. In contrast, (MeBr-DCNQI)₂Cu, as a function of temperature, shows a sharp change in reflectivity from the plane perpendicular to the *c* axis, and a gradual change along the *c* axis due to a gradual CDW formation along the *c* axis established earlier.⁹

IV. CONCLUSION

We have performed photoelectron and Auger electron spectroscopies for *in situ* synthesized (DMe-DCNQI)₂Cu

and (MeBr-DCNQI)₂Cu. From the photon-energy dependence using synchrotron radiation, we could successfully assign each observed feature in the valence-band photoemission spectra: the C and N 2*p* states originating in the quinone ring appear around 7.5 eV, and the primarily Cu 3*d* states mixed with the C and N 2*p* states of the cyano group are located around 3–4 eV in binding energy. The Br 4*p* states in (MeBr-DCNQI)₂Cu is also observed around 4.5 eV in binding energy. While the feature at the Fermi level is primarily derived from π -bonded C and N 2*p* states, the Cu 3*d* contribution at the Fermi level is larger in (MeBr-DCNQI)₂Cu compared to (DMe-DCNQI)₂Cu. X-ray photoemission spectra of the valence band imply extensive hybridization of the Cu 3*d* states, with C and N 2*p* states near the Fermi level. Line-shape analyses of the Cu 2*p* core-level spectra show that the ratio of Cu²⁺ to Cu⁺ is higher in (MeBr-DCNQI)₂Cu compared to (DMe-DCNQI)₂Cu, with the ratio being closer to 1:2. From a comparison of Cu *L*VV and C *K*VV Auger spectra with the self-convolution of the valence-band spectra, it was found that the effective on-site Coulomb correlation energies between the valence electrons are high on C as well as Cu sites in both salts,

with $U(pp)=6.5$ eV and $U(dd)=8.0$ eV, respectively. In conjunction with core-level spectra, the spectra indicate that the on-site Coulomb correlation, the hybridization strength, and the charge-transfer energy between the Cu 3*d* and N 2*p* ligands are very similar in both salts. The MI transition in the (MeBr-DCNQI)₂Cu is then facilitated by the proximity of the Cu²⁺ to Cu⁺ ratio to 1:2 supporting charge disproportion, while deviation from it stabilizes the metallic phase in the (DMe-DCNQI)₂Cu down to considerably low temperatures.

ACKNOWLEDGMENTS

We are grateful to H. Kobayashi of Toho University for providing high-purity neutral DMe-DCNQI and MeBr-DCNQI powders. We thank A. Fujimori and R. Kato of the University of Tokyo for useful discussions. We also thank T. Miura for help in the synchrotron-radiation photoemission measurement. A.C. thanks the Japan Society for the Promotion of Science for financial support. This work was supported by grants from New Energy and Industrial Technology Development Organization (NEDO) and the Ministry of Education, Science and Culture of Japan.

- ¹A. Aumuller, P. Erk, G. Klebe, S. Hunig, J. U. von Schutz, and H.-P. Werner, *Angew. Chem. Int. Ed. Engl.* **25**, 740 (1986).
- ²A. Kobayashi, R. Kato, H. Kobayashi, T. Mori, and H. Inokuchi, *Solid State Commun.* **64**, 45 (1987).
- ³R. Kato, H. Kobayashi, A. Kobayashi, Y. Mori, and H. Inokuchi, *Chem. Lett.* **1987**, 1579.
- ⁴A. Kobayashi, T. Mori, H. Inokuchi, R. Kato, and H. Inokuchi, *Synth. Met.* **27**, B275 (1988).
- ⁵T. Mori, H. Inokuchi, A. Kobayashi, R. Kato, and H. Kobayashi, *Phys. Rev. B* **38**, 5913 (1988).
- ⁶R. Kato, H. Kobayashi, and A. Kobayashi, *J. Am. Chem. Soc.* **111**, 5224 (1989).
- ⁷H. Kobayashi, A. Miyamoto, H. Morikawa, R. Kato, and A. Kobayashi, *Chem. Lett.* **1991**, 863.
- ⁸G. Lunardi and C. Pecile, *J. Chem. Phys.* **95**, 6911 (1991).
- ⁹H. Kobayashi, A. Miyamoto, R. Kato, F. Sakai, A. Kobayashi, Y. Yamakita, Y. Furukawa, M. Tatsumi, and T. Watanabe, *Phys. Rev. B* **47**, 3500 (1993).
- ¹⁰H. Kobayashi, R. Kato, A. Kobayashi, Y. Nishio, K. Kajita, and W. Sasaki, *J. Phys. Chem. Solids* **51**, 533 (1990).
- ¹¹S. Aonuma, H. Sawa, R. Kato, and H. Kobayashi, *Chem. Lett.* **1993**, 513.
- ¹²M. Tamura, H. Sawa, S. Aonuma, R. Kato, and M. Kinoshita, *J. Phys. Soc. Jpn.* **63**, 429 (1994).
- ¹³A. Tanaka, A. Chainani, T. Miura, T. Takahashi, T. Miyazaki, S. Hasegawa, and T. Mori, *Solid State Commun.* **93**, 1 (1995).
- ¹⁴J. J. Yeh and I. Lindau, *At. Data Nucl. Data Tables* **32**, 1 (1985).
- ¹⁵W. Koch and F. F. Seeling, *Z. Naturforsch.* **42a**, 875 (1987).
- ¹⁶D. Schmeißer, A. Gonzales, J. U. von Schutz, H. Wachtel, and H. C. Wolf, *J. Phys. (France) I* **1**, 1347 (1991).
- ¹⁷D. Schmeißer, P. Batz, W. Gopel, W. Jaegermann, Ch. Pottenkofer, H. Wachtel, A. Jimenez-Gonzales, J. U. von Schutz, H. C. Wolf, J. Taborski, V. Wustenhagen, E. Umbach, P. Erk, H. Meixner, and S. Hunig, *Ber. Bunsenges. Phys. Chem.* **95**, 1441 (1991).
- ¹⁸D. Schmeißer, K. Graf, W. Gopel, J. U. von Schutz, P. Erk, and S. Hinig, *Chem. Phys. Lett.* **148**, 423 (1988).
- ¹⁹D. Schmeißer, W. Gopel, U. Langohr, J. U. von Schutz, and H. C. Wolf, *Synth. Met.* **41-43**, 1805 (1991).
- ²⁰I. H. Inoue, M. Watanabe, T. Kinoshita, A. Kakizaki, R. Kato, A. Kobayashi, H. Kobayashi, and A. Fujimori, *Phys. Rev. B* **47**, 12917 (1993).
- ²¹W. D. Grobman, R. A. Polla, D. E. Eastman, E. T. Maas, Jr., and B. A. Scott, *Phys. Rev. Lett.* **32**, 534 (1974).
- ²²P. Nielsen, A. J. Epstein, and D. J. Sandman, *Solid State Commun.* **15**, 53 (1974).
- ²³B. Dardel, D. Malterre, M. Grinoi, P. Weibel, and Y. Baer, *Phys. Rev. Lett.* **67**, 3144 (1991).
- ²⁴S. Uji, *Parity* **9**, 40 (1994) (in Japanese).
- ²⁵S. Uji, T. Terashima, H. Aoki, J. S. Brooks, R. Kato, H. Sawa, S. Aonuma, M. Tamura, and M. Kinoshita, *Phys. Rev. B* **50**, 15597 (1994).
- ²⁶I. H. Inoue, A. Kakizaki, H. Namatame, A. Fujimori, A. Kobayashi, R. Kato, and H. Kobayashi, *Phys. Rev. B* **45**, 5858 (1992).
- ²⁷I. H. Inoue, A. Kakizaki, A. Kobayashi, R. Kato, H. Kobayashi, H. Namatame, and A. Fujimori, *Physica C* **185-189**, 2691 (1991).
- ²⁸J. Ghijsen, L. H. Tjeng, J. van Elp, H. Eskes, J. Westerink, G. A. Sawatzky, and M. T. Czyzyk, *Phys. Rev. B* **38**, 11322 (1988), and references therein.
- ²⁹D. A. Shirley, *Chem. Phys. Lett.* **17**, 312 (1972).
- ³⁰R. Hoogewijs, L. Fiermans, and L. Vennik, *Chem. Phys. Lett.* **38**, 471 (1976).
- ³¹P. Humbert and J. P. Deville, *J. Phys. C* **20**, 4679 (1987).
- ³²S. R. Barman and D. D. Sarma, *J. Phys. Condens. Matter* **4**,

- 7607 (1992), and references therein.
- ³³D. van der Marle, J. van Elp, G. A. Sawatzky, and D. Heitman, *Phys. Rev. B* **37**, 5136 (1988).
- ³⁴D. Schmeißer, W. Gopel, H. Fuchs, K. Graf, and P. Erk, *Phys. Rev. B* **48**, 4891 (1993).
- ³⁵H. Fukuyama, *Physica B* **199-200**, 656 (1994).
- ³⁶H. Sawa, M. Tamura, S. Aonuma, M. Kinoshita, and R. Kato, *J. Phys. Soc. Jpn.* **63**, 4302 (1994).
- ³⁷H. Tajima, G. Ojima, T. Ida, H. Kuroda, A. Kobayashi, R. Kato, H. Kobayashi, A. Ugawa, and K. Yakushi, in *The Physics and Chemistry of Organic Superconductors*, edited by G. Saito and S. Kagoshima (Springer-Verlag, Berlin, 1990), p. 49.